Structural and optical properties of magnetron sputtered $Mg_xZn_{1-x}O$ thin films

2006 J. Phys.: Condens. Matter 18 3343

(http://iopscience.iop.org/0953-8984/18/13/002)

INSTITUTE OF PHYSICS PUBLISHING JOURNAL OF PHYSICS: CONDENSED MATTER

J. Phys.: Condens. Matter **18** (2006) 3343–3354 doi:10.1088/0953-8984/18/13/002

Structural and optical properties of magnetron sputtered $Mg_xZn_{1-x}O$ thin films

Sanjeev Kumar[1], **Vinay Gupte and K Sreenivas**

Department of Physics and Astrophysics, University of Delhi, Delhi-110007, India

E-mail: sanjeev@scientific.net

Received 14 October 2005, in final form 22 January 2006
Published 13 March 2006
Online at stacks.iop.org/JPhysCM/18/3343

Abstract

$Mg_xZn_{1-x}O$ (MZO) thin films prepared by an rf magnetron sputtering technique are reported. The films were grown at room temperature and at relatively low rf power of 50 W. MZO thin films were found to possess preferred *c*-axis orientation and exhibited hexagonal wurtzite structure of ZnO up to a Mg concentration of 42 mol%. A small variation in the *c*-axis lattice parameter of around 0.3% was observed with increasing Mg composition, showing the complete solubility of Mg in ZnO. The band gap of the MZO films in the wurtzite phase varied linearly with the Mg concentration and a maximum band gap ∼4.19 eV was achieved at $x = 0.42$. The refractive indices of the MgO films were found to decrease with increasing Mg content. The observed optical dispersion data are in agreement with the single oscillator model. A photoluminescence study revealed a blue shift in the near band edge emission peak with increasing Mg content in the MZO films. The results show the potential of MZO films in various opto-electronic applications.

1. Introduction

Recent advances in the growth of wide band gap semiconducting oxide materials like ZnO has stimulated intense research, and efforts are focused on studying the influence of different dopants on their multifunctional properties. These doped oxides exhibit properties that are either enhanced or are entirely new [1–3]. $Mg_xZn_{1-x}O$ (MZO) has emerged as one of the promising compound semiconductors which is formed when Mg is alloyed with ZnO. ZnO, which belongs to the wurtzite family, is a well known piezoelectric material, and alloying with MgO, which is non-piezoelectric and has the cubic rock salt structure, is reported to yield beneficial properties for piezoelectric device applications [4]. The composition of Mg in the MZO alloy determines the crystallographic structure, which can be tailored from wurtzite phase of ZnO to the cubic phase of MgO [1, 5, 6]. If the structural differences are ignored, then the

[1] Author to whom any correspondence should be addressed.

optical band gap of the MZO alloy can be tuned from 3.3 to 7.8 eV depending upon the Mg content ($0 \leqslant x \leqslant 1.0$) [7]. The enhanced optical band gap of the MZO alloy has been successfully exploited to sense mid and deep ultraviolet (UV) light [7]. Thus, the growth of wurtzite MZO films is expected to find potential applications in novel acousto-optic and acousto-electric devices besides its application for optical devices in the UV region.

According to the binary phase diagram, the solid solubility of MgO in ZnO is reported to be less than 4 mol%, whereas that of ZnO in MgO is around 40–50% [8, 9]. The limit of solubility of Mg in ZnO is found to depend largely on the deposition techniques and the processing conditions. MZO films have been grown by a variety of techniques such as pulse laser deposition (PLD), metal-organic chemical vapour deposition (MOCVD), metal-organic vapour phase epitaxy (MOVPE), reactive electron-beam evaporation deposition (REBED), spray pyrolysis, co-sputtering, and molecular beam epitaxy (MBE) [4–7, 10–15]. Deposition techniques like PLD have shown a solubility limit of 33 mol% of Mg in ZnO [1, 5–7]; however, the MZO films grown by MOVPE and co-sputtering have shown an enhanced solubility of 49 and 46 mol% respectively [10, 13]. Much of the earlier reported work focused on using an epitaxially matched substrate like sapphire and high processing temperature (250–750 °C) [1, 5, 10–12]. Amongst the various deposition techniques, rf magnetron sputtering offers a cold deposition process and it can be scaled up easily to provide deposited films over a large area. The realization of optical devices requires detailed information on optical constants such as the refractive index of film material, and only a few reports [11, 16] have described the optical properties of the MZO films. However, the optical properties of rf magnetron sputtered MZO films deposited on unheated substrates have not yet been reported.

In the present work, the growth and characterization of wurtzite $Mg_xZn_{1-x}O$ thin films ($x \leqslant 0.42$) using an rf magnetron sputtering technique on fused quartz and normal glass slides at room temperature is reported, and the optical and structural properties of MZO films with varying Mg composition have been studied.

2. Experimental details

$Mg_xZn_{1-x}O$ thin films were grown on 1 inch fused quartz (FQ) wafers and normal soda lime glass slides using an rf magnetron sputtering technique. The MZO target was made by placing 1 cm diameter Mg (99.99%) discs on the surface of a 4 inch Zn(99.99%) metal target. The magnetron electrode was installed on the base plate of the sputtering chamber, which provided the capability to hold the MZO target with a copper backing plate on the magnetron electrode. The substrates were cleaned thoroughly using trichloroethylene, acetone and propanol respectively, and were finally cleaned in a vapour degreasing equipment with isopropyl alcohol for 24 h. The substrate to target distance was 7.5 cm. The chamber was pumped down to a high vacuum of 10^{-6} mTorr, and the MZO films were deposited in a reactive gas ambient of $Ar:O_2$ (50:50) at 10 mTorr sputtering pressure at an applied rf power of 50 W. The rate of deposition for the MZO thin films was found to be 100 nm h^{-1}, and was low in comparison to ZnO films (500 nm h^{-1}) under similar deposition conditions. All the depositions were done without any substrate heating.

The deposited MZO films were characterized for phase and crystallographic orientation using an x-ray diffraction (XRD) technique. Atomic force microscopy (AFM) was utilized to study the surface morphology and the roughness of the grown films. UV–visible spectroscopy was utilized for studying the optical transparency and absorption, and for the evaluation of the band gap and refractive indices. Photoluminescence (PL) studies were performed on the MZO alloys to study the change in emission peaks with varying Mg concentration. X-ray photoelectron spectroscopy (XPS) was used to study the chemical composition of the deposited MZO films.

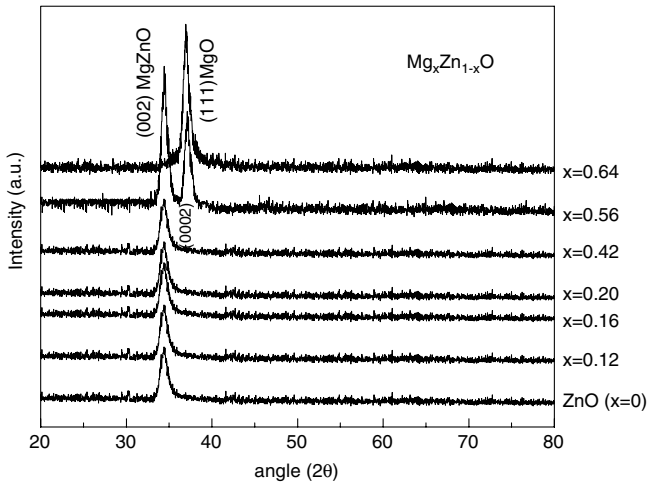

Figure 1. XRD profile of $Mg_xZn_{1-x}O$ thin films ($0 \leqslant x \leqslant 0.64$) showing the phase segregation after $x = 0.42$.

3. Results and discussions

3.1. Structural and surface morphological studies

Figure 1 shows the XRD patterns observed from $Mg_xZn_{1-x}O$ (MZO) films deposited on FQ substrates. Undoped ZnO films ($x = 0$) exhibited a preferred orientation along the (0002) plane, showing the crystallographic hexagonal wurtzite structure. Mg alloyed ZnO films ($x \leqslant 0.42$) showed a single peak corresponding to the (0002) plane of ZnO, and these films exhibited a crystallographic structure similar to that of pure ZnO. However, at higher Mg content ($x = 0.56$) two peaks corresponding to the (002) plane of ZnO and (111) plane of MgO are observed, indicating the onset of phase segregation of MgO from the lattice site of the MZO. The (002) peak of MZO films completely disappeared with further increasing Mg content to 64 mol% and a single peak at $2\theta = 36.8°$ is reflected in the XRD spectra that corresponds to the (111) plane of the cubic MgO rock salt structure. This clearly indicates a phase transformation of MZO films from crystallographic wurtzite to cubic structure. However, the structural phase transition is not abrupt, and a mixed phase for the intermediate values of x ($0.42 < x < 0.64$) was observed, as is evident from the XRD spectra (figure 1). Similar observations on the appearance of phase segregation have been reported earlier, and the Mg content in the MZO where the onset of phase segregation is observed is found to vary considerably [10, 13]. According to the binary phase diagram of MgO–ZnO, the thermodynamic solid solubility limit of MgO in wurtzite ZnO is less than 4% [8]. Therefore, the films that are produced with Mg concentration greater than 4 mol% can be considered to be thermodynamically unstable due to the establishment of a non-equilibrium state between the cubic MgO and wurtzite ZnO phases and remain in metastable phase [1]. However, Ohtomo *et al* [1] found that MZO films deposited by the PLD technique with 33 mol% Mg concentration were thermodynamically stable and remain in a single state. Similar results have been reported by other workers; however, the solubility limit of Mg in ZnO is invariably reported to differ, and depends on the processing technique and the growth parameters [5–7, 10–12]. Park *et al* [10] obtained a stable MZO alloy up to a thermodynamic limit of 49 mol% and attributed the extended limit in the solubility to the low temperature growth conditions employed for the films grown by MOVPE.

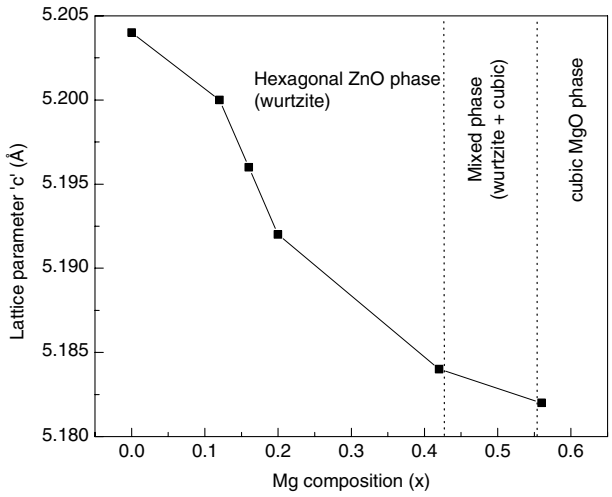

Figure 2. Variation of *c*-axis lattice parameter with Mg concentration in MZO films.

Yang *et al* [7] reported that with an increase in the substrate temperature the Mg content in the cubic phase of MZO alloy deposited by PLD was found to increase due to the high desorption rate of Zn, resulting in Mg-rich films. Thus higher substrate temperature is seen to result in a poor control of the Mg composition in the growing MZO film. The low temperature growth together with a low sputtering power, adopted in the present work, resulted in a higher thermodynamic solubility of Mg in ZnO (up to 42 mol%) and the alloy film remains in a single phase and is in close agreement with the observations of Minemoto *et al* [13], who reported a solubility limit of 46 mol% for MZO films prepared by co-sputtered ZnO and MgO targets.

It is observed that the position of the peak corresponding to the (0002) plane of the wurtzite phase in the XRD spectra of the MZO films is shifted to higher diffraction angle with increasing Mg concentration. These observations are in agreement with the earlier reports [10, 13] on MZO films deposited by other techniques and indicate a decrease in the *c*-axis lattice parameter of the MZO films due to Mg incorporation. The variation of the *c*-axis lattice parameter as a function of the Mg concentration is shown in figure 2. It may be noted that the change in *c*-axis lattice parameter is very small (0.3%) as compared to the earlier reports, where 1.34% [10] and 0.9% [15] changes have been reported in the *c*-axis. Since the ionic radius of Zn^{2+} (0.60 Å) and Mg^{2+} (0.57 Å) are almost similar, the substitution of Mg^{2+} at the Zn^{2+} lattice site under low processing temperature results in an insignificant change in the unit cell dimension as long as the Mg does not segregate from the unit cell of ZnO. The lattice parameters are expected to be influenced by the defects present at the interstitial sites. Therefore, a large variation in the *c*-axis lattice parameter observed by other workers may be due to the incorporation of Mg at the interstitial sites of the MZO films. A small change in the *c*-axis lattice parameter in the present study suggests that magnetron sputtered Mg-doped ZnO films are more thermodynamically stable in comparison to other techniques and the possibility of MgO segregation is low when films are deposited on unheated substrates and at low rf sputtering power.

Figure 3(a) shows a scanning electron micrograph of MZO film ($x = 0.20$) deposited on fused quartz substrates. The surface of the MZO films was highly dense and smooth. The SEM micrograph shows that the films were nanocrystalline, which is also confirmed by the atomic force microscopy. Figure 3(b) shows the AFM imaged picture of the surface of deposited $Mg_xZn_{1-x}O$ film with $x = 0.20$, showing the surface to be highly smooth. The average

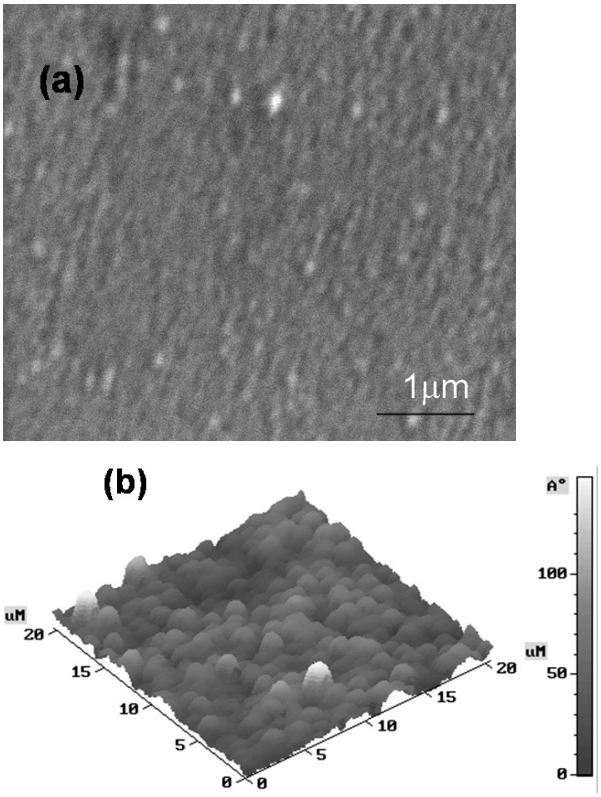

Figure 3. (a) SEM micrograph of $Mg_xZn_{1-x}O$ ($x = 0.20$) showing the dense microstructure; (b) AFM image of $Mg_xZn_{1-x}O$ ($x = 0.20$) thin film depicting well developed grains. The average roughness of the MZO films was estimated to be ∼5 nm ($x \leqslant 0.42$).

surface roughness of the undoped ZnO films was around 3 nm, which increased to ∼5 nm with increasing Mg content in the MZO films with $x \leqslant 0.42$. However, a sudden increase in the average roughness to 15 nm was observed for MZO films with 56 mol% Mg content. The variation of the surface roughness can be attributed to difference in the sputtering rate of MgO and ZnO.

3.2. Optical studies

3.2.1. UV–visible transmission. The Mg incorporation well into the crystallites of the ZnO reflected a systematic variation in the UV–visible transmission spectra of MZO films with increasing Mg composition. Figure 4 shows the transmittance spectra obtained on various compositions of MZO films at room temperature. The absorption edge is found to shift to lower wavelengths with increasing Mg content in the films. All the films exhibited a sharp absorption and the optical transparency was more than 85%. It may be noted that no significant variation in transmittance was observed in the visible range with increasing Mg concentration in the MZO films. This suggests that scattering defect centres remain unaffected with increasing Mg concentration in the range $0 \leqslant x \leqslant 0.42$. This result verifies the optically high quality of the MZO films. It is interesting to note that all the compositions exhibited a sharp absorption edge, whereas in the earlier reported studies [13, 17] at higher Mg composition a broadening

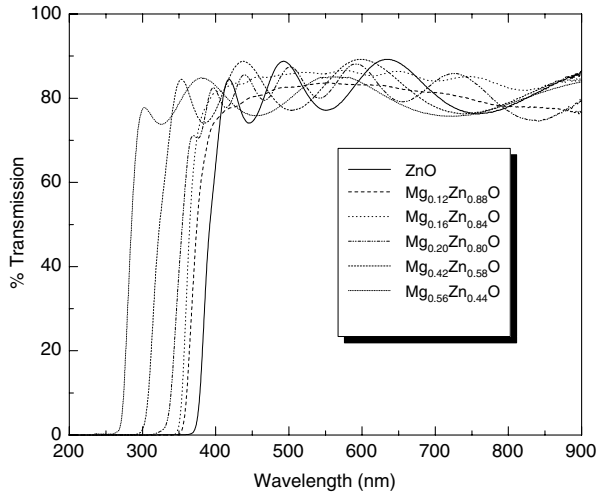

Figure 4. UV–visible transmission spectra of $Mg_xZn_{1-x}O$ thin films ($0 \leqslant x \leqslant 0.56$) grown on fused quartz substrates.

in the absorption edge is normally observed and is attributed to the Mg segregation from the lattice site of MZO films [13, 17]. In the present work, no such broadening was observed in the sputtered MZO films, and this is in agreement with the XRD analysis as shown in figure 1. Since all the MZO films exhibited a sharp absorption edge, it is difficult to predict the possibility of any indirect transition. With experience, and common observations indirect transitions are seen when the absorption fall is shallow. For example, in the case of an indirect band gap semiconductor like GaSe, the absence of sharp absorption and the broadening of the absorption edge reinforce the notion of an indirect transition [18]. However, in the present work, no broadening of the absorption edge was observed at all, and this indicates the occurrence of a direct band transition in the MZO films prepared in the present work.

The other way to find the direct or indirect transition in a crystalline or polycrystalline material is to determine the relation between the absorption coefficient (α) and the optical energy gap (E_g). Assuming the band gap to be parabolic in nature, the absorption coefficient in the case of a direct transition is related to the band gap by

$$\alpha h\nu = \text{const}(h\nu - E_g)^n \tag{1}$$

and in the case of an indirect transition it is given by

$$\alpha h\nu = A\frac{(h\nu - E_g + E_p)^n}{\exp(\theta_D/T) - 1} + B\frac{(h\nu - E_g - E_p)^n}{1 - \exp(-\theta_D/T)} \tag{2}$$

where A and B are constants, E_p is the phonon energy, θ_D is the Debye temperature, and n takes on different values [19] such as $n = 1/2$ for a direct allowed transition, $n = 1/3$ for a direct forbidden (in the quantum mechanical sense) transition, $n = 2$ for an indirect transition, $n = 3$ for an indirect transition.

The method to calculate the band gap is to plot a graph between $(\alpha h\nu)^{1/n}$ and $h\nu$ and find the value of n which gives the best linear graph. This value of n decides the nature of the energy gap or transition involved. In the case of direct band gap materials, the graph shows a linear portion which is extrapolated, and the intercept on the $h\nu$ axis gives the value of band gap, E_g. In the present work, the value of n was varied, and it was found that at $n = 1/2$, the graph between $(\alpha h\nu)^{1/n}$ and $h\nu$ is a linear curve for all compositions. Figure 5 shows the plot of

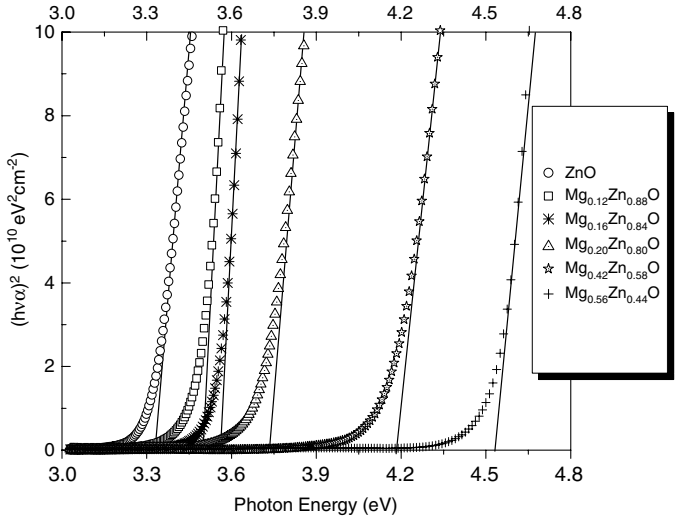

Figure 5. Plot of square of absorption coefficient versus photon energy for $Mg_xZn_{1-x}O$ films ($0 \leqslant x \leqslant 0.56$).

$(\alpha h\nu)^2$ as a function of photon energy $(h\nu)$; the band gap was determined by extrapolating the $(h\nu)$ intercept. Figure 6 shows the variation of band gap of the MZO films as a function of Mg content. It can be seen that the band gap of the MZO films varies almost linearly with increasing Mg content in the films up to $x = 0.56$, and beyond this composition a sudden increase in band gap was observed. A comparison of the present data with the earlier reports (figure 6) shows that the observed variation is in close agreement with the data of Minemoto *et al* [13] on MZO films produced by co-sputtering. It may also be noted that the variation of band gap with Mg content is different for the sputtered and the laser ablated films (figure 6). The band gap data for PLD films having wurtzite structure were taken from the reported data of Ohtomo *et al* [1], and those for MZO films having cubic structure were taken from the reported data of Choopun *et al* [5]. It is interesting to note that in wurtzite phase MZO films grown by PLD and sputtering showed a similar band gap variation (for $x \leqslant 0.33$). However, with a higher Mg content ($x \sim 0.45$), PLD films showed a slightly higher value of band gap (4.94 eV) in comparison to the sputtered films (4.21–4.27 eV). This may be attributed due to the thermodynamic non-equilibrium nature of the PLD films [1]. Furthermore, in the PLD system the film growth is usually done at higher substrate temperature, and thereby the concentration of Mg in the deposited films is reported to be high [7], and Mg may be incorporated at the interstitial sites and the grain boundaries. These observations are in fairly good agreement with the observed broadening in the absorption edge of the MZO films deposited by PLD [10]. In the present study, the maximum achievable band gap of the RF magnetron sputtered MZO films having wurtzite structure was 4.19 eV at Mg concentration of 42 mol%.

3.2.2. Refractive index. The index of refraction, $n(\lambda)$, at different wavelengths was calculated by the Manifacier method [20] using the following formula:

$$n = [N + (N^2 - n_0^2 n_1^2)^{1/2}]^{1/2} \tag{3}$$

where

$$N = \frac{(n_0^2 + n_1^2)}{2} + 2n_0 n_1 \frac{(T_{\max} - T_{\min})}{T_{\max} T_{\min}}. \tag{4}$$

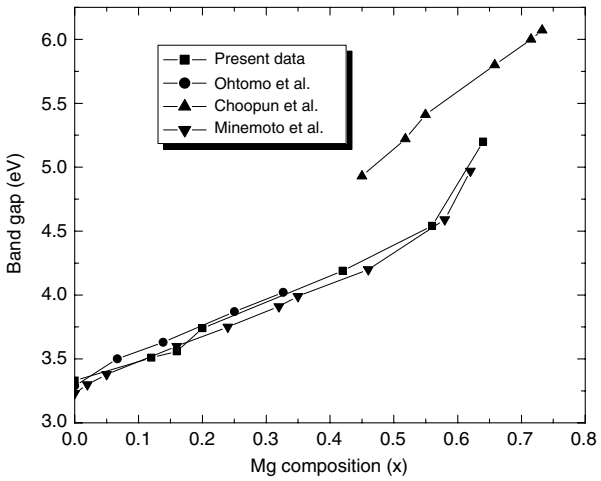

Figure 6. Plot showing the variation of band gap with Mg content in $Mg_xZn_{1-x}O$ thin films. For comparison the reported data of MZO films deposited by PLD and sputtering are also shown.

n_0 and n_1 are the refractive indices of the air and the fused quartz substrate. Here T_{max} and T_{min} are maxima and minima obtained by the envelope method in the transmission curve of the MZO films, and are functions of λ. The refractive indices of the MZO films are calculated as a function of Mg composition and are shown in figure 7. For comparison the refractive indices of MZO and MgO films deposited by PLD are also shown. It may noted that the variation of refractive indices is in close proximity with the refractive indices reported earlier on films deposited by other techniques (figure 7). A systematic decrease in refractive index of the deposited MZO films was observed with increase in Mg concentration. Figure 8 illustrates the variation of refractive index of MZO film at $\lambda = 700$ nm and c-axis lattice parameter with Mg composition. It is interesting to note that the refractive index varies in accordance with the c-axis, indicating some correlation between the optical and structural properties of MZO films. The decrease in refractive index of the MZO films may be attributed to a decrease in the c-axis lattice parameter with increasing Mg concentration. These results are in agreement with the observations of Dietrich *et al* [21], where they observed a decrease in refractive index with a change in the lattice parameter for a tin-doped indium oxide films.

3.2.3. Optical dispersion. Figure 7 shows the frequency dispersion of the refractive indices of MZO films at various Mg compositions. The frequency dispersion of refractive index has been extensively studied using the single oscillator model which can be expressed as [22]

$$n^2 - 1 = \frac{E_d E_0}{E_0^2 - (h\nu)^2} \tag{5}$$

where $h\nu$ is the photon energy, E_0 is the single oscillator energy, and E_d is the dispersion energy. E_d is a measure of the strength of inter-band optical transitions, and can be defined as

$$E_d = \beta N_c Z_a N_e \tag{6}$$

where N_c is the coordination number of the cation nearest neighbour to the anion, Z_a is the valency of the anion, N_e is the effective number of valence electrons per anions, and β is two valued, taking on ionic values for oxides, and covalent values for zinc blende, diamond structures, etc. The obtained data of the refractive indices are theoretically fitted to the single

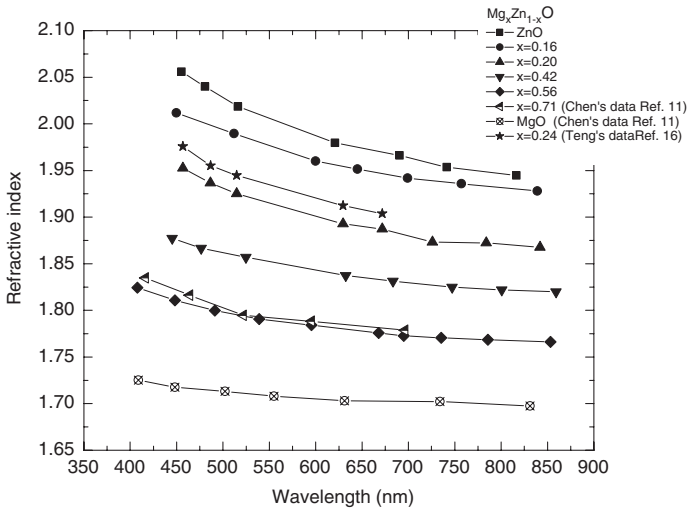

Figure 7. Variation of refractive indices of $M_xZn_{1-x}O$ thin films ($x = 0, 0.16, 0.20, 0.42, 0.56$) with photon energy. The plot also shows the data of earlier reported wurtzite [16] and cubic [11] MZO films grown by PLD.

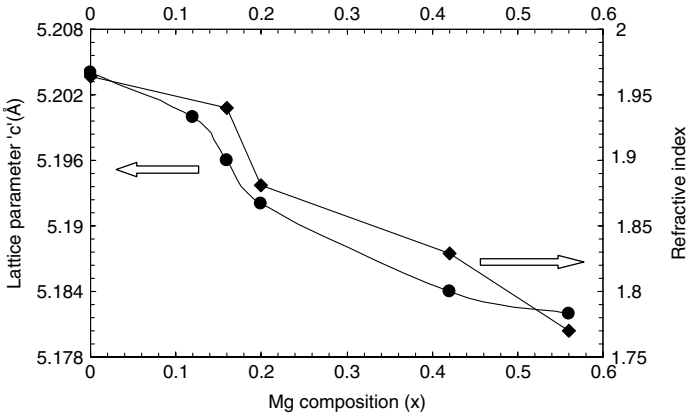

Figure 8. Variation of c-axis lattice parameter and refractive index ($\lambda = 700$ nm) with Mg composition in the $Mg_xZn_{1-x}O$ ($0 \leqslant x \leqslant 0.56$).

oscillator model using equation (5), and the experimentally observed dispersion is found to be in agreement with the single oscillator fit, and is shown in figure 9. Table 1 lists the values of fitting parameters E_0 and E_d estimated for MZO films with varying Mg composition. The values of E_0 and E_d are close to the range reported for ZnO and MgO materials.

Another interesting parameter is β (equation (4)), which takes ionic values $\sim$0.26 $\pm$ 0.04 eV for most of the oxides. For the wurtzite crystal structure (ZnO) values of N_c, Z_a, and N_a are 4, 2, and 8 respectively, and for cubic oxides (like MgO) N_c, Z_a, and N_a take the values 6, 2, and 8, respectively [22]. Using theses values, β is calculated and listed in table 1. It may be noted that the values of β obtained for the sputtered MZO films in the present study are in the range reported for the ionic class of materials.

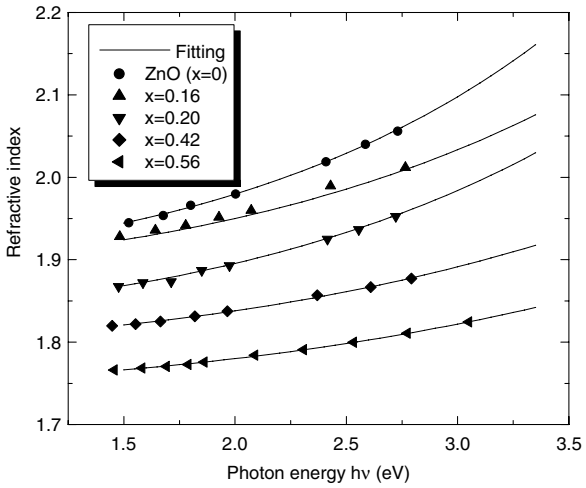

Figure 9. Frequency dispersion of refractive index of $Mg_xZn_{1-x}O$ films with different Mg compositions. The solid curve represents the dispersion obtained by fitting with the single oscillator model.

Table 1. Fitting parameters for the single oscillator model.

Mg content (mol%)	E_0 (eV)	E_d (eV)	β (eV)
0	6.27	16.44	0.26
16	6.84	16.22	0.25
20	7.16	18.16	0.28
42	8.29	18.53	0.29
56	8.99	18.56	0.29
ZnO[a]	6.40	17.10	0.27
MgO[a]	11.30	22.0	0.23

[a] Reference [22].

4. Blue shift in luminescence spectra

Figure 10 shows the photoluminescence spectra taken at room temperature of the MZO films with different Mg concentration. The luminescence peak of the pure ZnO was observed at 373 nm, which decreased to 364 and 302 nm at Mg concentration of 12 mol% and 42 mol%, respectively. It may be noted that in all films near band edge (NBE) emission was observed, and no peaks corresponding to deep level emission were observed. A small broadening at deep levels is normally observed for ZnO films with zinc or oxygen defects [23]. However, in the present work, there could be some defects in the films that may be non-emissive; therefore, the presence of defects in the films cannot be completely ruled out. It is found that peaks of the NBE emission of MZO films showed a blue shift to higher energies with increasing Mg content. The PL peak corresponding to pure ZnO film is narrow, and a small broadening is observed in the MZO films at lower wavelength values (figure 10). The broadening of the luminescence peaks is normally observed in an alloy semiconductor [1], where charge carriers observe different potentials depending on the local concentration and also on the arrangements of the substituting elements. This effect is larger in ZnO as the Bohr radius of the excitons in ZnO is as small as 18 Å, and therefore the excitons are more sensitive to local inhomogeneity [1].

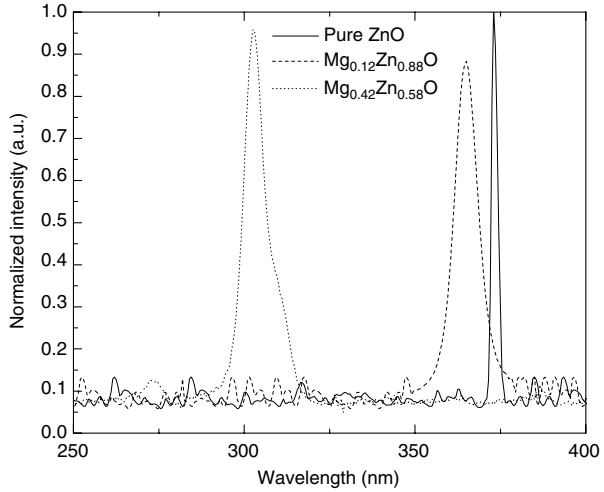

Figure 10. Photoluminescence spectra of $Mg_xZn_{1-x}O$ thin films at different Mg compositions ($x = 0, 0.12, 0.42$) showing blue shift of the emission peaks to lower wavelength with increasing Mg composition.

5. Conclusions

In conclusion, high quality $Mg_xZn_{1-x}O$ thin films have been grown on unheated fused quartz substrate by rf magnetron sputtering. The $Mg_xZn_{1-x}O$ films retain the wurtzite hexagonal structure of ZnO and a thermodynamic solubility limit is achieved up to a Mg concentration of 42 mol%, where the band gap of the alloy is 4.19 eV. The variation in c-axis lattice parameter is very small for $Mg_xZn_{1-x}O$ films and shows excellent thermodynamic stability. The refractive indices of MZO films were found to decrease with increase in Mg concentration, and the optical dispersion data fit well to the single oscillator model. The blue shift in the near band edge (NBE) emission peak with increasing Mg content indicates that rf magnetron sputtered MZO films can be used not only for deep UV light detection, but also for highly efficient deep UV lasing applications.

Acknowledgments

One of the authors (SK) wishes to thank CSIR, India for the award of a research fellowship (SRF), and would like to thank the reviewers of this manuscript for the scintillating discussions.

References

[1] Ohtomo A, Kawasaki M, Koida T, Masubuchi K, Koinumpa H, Sakurai Y, Yoshida Y, Yasuda T and Segawa Y 1998 *Appl. Phys. Lett.* **72** 2466
[2] Sharma P, Gupta A, Rao K V, Owens F J, Sharma R, Ahuja R, Gullen J M O, Johansson B and Gehring G A 2003 *Nat. Mater.* **2** 673
[3] Makino T, Segawa Y, Kawasaki M, Ohtomo A, Shiroki R, Tamura K, Yasuda T and Koinuma H 2001 *Appl. Phys. Lett.* **78** 1237
[4] Emanetoglu N W, Muthukumar S, Wu P, Wittstruck R W, Chen Y and Lu Y 2003 *IEEE Trans. Ultrason. Ferroelectr. Freq. Control* **50** 537
[5] Choopun S, Vispute R D, Yang W, Sharma R P, Venkatesan T and Shen H 2002 *Appl. Phys. Lett.* **80** 1529
[6] Narayan J, Sharma A K, Kvit A, Jin C, Muth J F and Holland O W 2002 *Solid State Commun.* **121** 9

[7] Yang Y, Hullavard S S, Nagaraj B, Takeuchi I, Sharma R P, Venkatesan T, Vispute R D and Shen H 2003 *Appl. Phys. Lett.* **82** 3424
[8] Segnit E R and Holland A E 1965 *J. Am. Ceram. Soc.* **48** 409
[9] Hansson R, Hayes P C and Jak E 2004 *Scand. J. Metall.* **33** 355
[10] Park W I, Yi G-C and Jang H M 2001 *Appl. Phys. Lett.* **79** 2022
[11] Chen N B, Wu H Z and Xu T N 2005 *J. Appl. Phys.* **97** 023515
[12] Terasako T, Shirakata S and Kariya T 2002 *Thin Solid Films* **420/421** 13
[13] Minemoto T, Negami T, Nishiwaki S, Takakura H and Hamakawa Y 2000 *Thin Solid Films* **372** 173
[14] Hwang D-K, Jeong M-C and Myoung J-M 2004 *Appl. Surf. Sci.* **225** 217
[15] Ohtomo A, Kawasaki M, Sakurai Y, Ohkuba I, Shirok R, Yoshida Y, Yasuda T, Segawa Y and Koinuma H 1998 *Mater. Sci. Eng.* B **56** 263
[16] Teng C W, Muth J F, Özgür Ü, Bergmann M J, Everitt H O, Sharma A K, Jin C and Narayan J 2000 *Appl. Phys. Lett.* **76** 979
[17] Sharma A K, Narayan J, Muth J F, Teng C W, Jin C, Kvit A, Kolbas R M and Holland O W 1999 *Appl. Phys. Lett.* **75** 3327
[18] Besson J M *et al* 1974 *Phys. Rev. Lett.* **32** 936
[19] Seeger K 1973 *Semiconductor Physics* (Berlin: Springer)
[20] Manifacier J C, Gasiot J and Fillard J P 1976 *J. Phys. E: Sci. Instrum.* **9** 1002
[21] Dietrich A, Schmalzbaur K and Hoffmann H 1984 *Thin Solid Films* **122** 19
[22] Wemple S H and DiDomenico M 1971 *Phys. Rev.* B **3** 1338
[23] Shan F K, Kim B I, Liu G X, Sohn J Y, Lee W J, Shin B C and Yu Y S 2004 *J. Appl. Phys.* **95** 4772